Cellulose (2023) 30:11737–11751
https://doi.org/10.1007/s10570-023-05617-7

ORIGINAL RESEARCH

Bacterial cellulose/silver composite film in-situ coated copper alginate for thermally responsive antimicrobial dressing

Baiqing Song · Tianyi Zhang · Xinfeng Li · Kaili Yang · Guangming Tian · Yunzhi Dang · Jianhua Ma

Received: 4 May 2023 / Accepted: 11 November 2023 / Published online: 22 November 2023

Abstract Intelligent, controlled, slow-release antimicrobial materials have shown excellent application prospects in the medical field. Herein, silver particles (Ag) were synthesized using the hydrothermal method and a bacterial cellulose (BC) membrane as a template. The BC/Ag composite membrane was clad with copper alginate (CAlg) via the in-situ dip-coating method. Based on the Cu^{2+} ions in copper alginate, a layer of copper sulfide (CuS) was formed through a liquid-phase sulphuration reaction. This CuS layer leads the film to possess a photothermal and electrothermal response. Furthermore, we systematically investigated the microstructure, mechanical strength, and antibacterial properties of the composite film. The tensile strength of the BC/Ag/CAlg/CuS sample can reach 14.7 MPa, which should be attributed to the combination of the Cu^{2+} cross-linked CAlg and the inner BC/Ag composite film. Meanwhile, this assembled film exhibited hydrophilic and hygroscopic properties, as the antibacterial Ag particles can be continuously released and migrated from the inner layer to the outer layer. Finally, the BC/Ag/CAlg/CuS film inhibited *Staphylococcus aureus* and *Escherichia coli* by 99.9% and 99.6%, respectively, which should be attributed to the synergistic effect of silver ions and CuS's electrical and photothermal stimulation responses. These characteristics of the thermally responsive BC/Ag composite films indicate that they may successfully serve as wound dressings and other medical biomaterials.

Keywords Bacterial cellulose · Alginate · Nano silver · Cupric sulfide · Antibacterial

Baiqing Song and Tianyi Zhang have contributed equally to this work.

Supplementary Information The online version contains supplementary material available at https://doi.org/10.1007/s10570-023-05617-7.

B. Song · T. Zhang · X. Li · K. Yang · G. Tian · J. Ma (✉)
School of Materials Science and Engineering, Xi'an Polytechnic University, Xi'an 710048, Shaanxi, China
e-mail: majianhua@xpu.edu.cn

B. Song
e-mail: 1106634216@qq.com

T. Zhang
e-mail: 449166169@qq.com

X. Li
e-mail: 2865578604@qq.com

K. Yang
e-mail: yangkaili0215@163.com

G. Tian
e-mail: tianguangming@mail.nwpu.edu.cn

Y. Dang
Department of Radiation Oncology, Shaanxi Provincial People's Hospital, Xi'an 710086, China
e-mail: dangyunzhi@xiyi.edu.cn

Introduction

As the immune system's first line of defense, the skin protects the human body's internal organs and acts as a physical and chemical barrier to prevent pathogen invasion and dehydration (Deng et al. 2021; Zheng et al. 2020; Pazyar et al. 2014). However, the patient will be exposed to bacterial infections, tissue dehydration, and severe secondary trauma once a skin injury occurs (Wen et al. 2020). Though wound healing occurs naturally, complications such as infection and inflammation often occur, and the appearance of infection is prevented clinically by using antibiotics (Su et al. 2017). Unfortunately, the use of antibiotics frequently leads to the development of bacterial resistance while eliminating bacterial infections (Durand et al. 2019). Therefore, an ideal wound-healing dressing with unique properties that can maintain a moist environment, possess excellent antibacterial activities, protect the wound from infections, absorb excess wound exudates, and allow gas exchange is highly demanded (Dart et al. 2019; Yang et al. 2017).

Silver, whether in nanoparticle (AgNPs), oxide (mainly Ag_2O), or ionic form (Ag^+), has shown excellent antibacterial activity (Lee et al. 2007; Rieger et al. 2016). It has long been used as a broad-spectrum antimicrobial agent against bacteria, fungi, and viruses. The advantage of AgNPs over other antimicrobial agents is their higher toxicity to microorganisms (Zhao et al. 2015; Nie et al. 2021a, b, c). Although some arguments exist about the potential cytotoxicity of the released silver ions, most studies have shown that silver is safe to use as an antimicrobial agent at the maximum allowable dose (Dos Santos et al. 2014; Wijnhoven et al. 2009). Yet, in the case of typical applications such as wound healing, it would be preferable to integrate AgNPs into a specific porous material and control the release of Ag^+ to improve their antibacterial durability (Tabaii et al. 2018). Bacterial cellulose (BC), synthesized by Acetobacter, is environmentally friendly. It has excellent characteristics such as high porosity, water absorption, mechanical properties, formability, and biocompatibility (Sulaeva et al. 2015). In addition, it is considered a natural wound dressing without changing its structure or properties. Hence, there is increasing interest in producing hybrid Ag/BC materials for antimicrobial treatments (Pal et al. 2017; Yang et al. 2012a, b, c; Liu et al. 2020; Nie et al. 2021a, b, c). Yang et al. used BC as a template for the in-situ synthesis of AgNPs by chemical reduction of sodium borohydride (Yang et al. 2012a, b, c). They found that abundant hydroxyl groups on BC microfibers acted as anchor sites for silver ions, the nanopores of BC materials served as nano-reactors for the nucleation and growth of AgNPs, limiting the growth of particles within the pores, and the prepared AgNPs became smaller in size and narrower in size distribution (Pinto et al. 2009; Wan et al. 2020). Even so, the antimicrobial composite films prepared using BC alone always suffer from poor mechanical strength in the wet state and weak water swelling ability after drying. To resolve this, many researchers tried to combine BC with inorganic filler or synthetic polymers, such as clay (Perotti et al. 2011) and PVA (Song et al. 2021a, b), but it is still hard to improve the mechanical strength and water swelling ability simultaneously for the composite film. Alginate (Alg), a natural linear, unbranched polymer made of 1,4-linked β-D-mannosic acid and α-L-guluronic acid, is widely used as biomedical material (Shen et al. 2022). Combining the water solubility, cross-linkability, and biocompatibility of alginate, many studies have prepared composites by mixing BC with Alg (Chiaoprakobkij et al. 2011; Jiang et al. 2020; Ji et al. 2021). Generally, researchers crushing BC matrix into slurry and mixing it with alginate solution, followed by coagulation with $CaCl_2$ (Wang et al. 2020). Unfortunately, the crosslinked BC/Alg composites usually exhibited a weaker mechanical strength than pure BC. This mechanical decrease might be attributed to the damage of BC's network microstructure (Siddhan et al. 2016). Herein, we intend to prepare BC/Alg dual network composites using BC films instead of BC slurry. This method is expected to maintain the natural three-dimensional network structure of BC, resulting in improved mechanical strength and water swelling capacity.

Currently, most dressings available on the market are gauze-based and incorporate antibiotics for antibacterial properties. However, the use of antibiotics not only sterilizes and reduces inflammation but also promotes the development of antibiotic resistance in certain bacteria, thereby diminishing the effectiveness of sterilization and inflammation reduction. In this work, we have developed CAlg-encapsulated BC/Ag antimicrobial films with a thermally responsive slow-release effect. Initially, BC/Ag film was

hydrothermally synthesized using BC as a template for the inner layer structure (Li et al. 2014). Subsequently, Alg was impregnated onto the surface of the BC/Ag film, forming an interpenetrating structure with the BC matrix, followed by additional Cu^{2+} cross-linking to construct the CAlg encapsulation layer. By employing the copper ions in CAlg, we selectively conducted a liquid-phase sulfide reaction on the external CAlg. As a result, a copper sulfide (CuS) layer was deposited in situ on the surface of the composite antimicrobial film. On the one hand, the CuS layer endows the composite film with excellent photothermal and electrothermal characteristics (Nie et al. 2021a, b, c); on the other hand, CuS also acts as an auxiliary antimicrobial component (Qiao et al. 2019; Ren et al. 2022; Mutalik et al. 2022). During the study, we systematically described the microstructure and physical properties of the composite film, as well as the antibacterial, photothermal, and electrothermal slow-release properties. The development of this study will provide a theoretical basis and experimental support for developing and applying high-performance bio-based antibacterial wound dressings.

Experimental section

Experimental materials

Bacterial cellulose was supplied from QiHong Technology Co Ltd (Guilin, China). Sodium alginate was purchased from Aladdin Reagents Ltd (Shanghai, China). Silver nitrate ($AgNO_3$), copper chloride ($CuCl_2$) and sodium sulphide (Na_2S) were purchased from Sinopharm Chemical Reagent Co Ltd (Shanghai, China). All the chemicals were in analytical grade and used without further purification.

Preparation of BC/Ag composite antimicrobial film

Synthesis of BC/Ag nanocomposite: BC in gel form was boiled in a solution of NaOH at pH 13 for 4 h at 110 °C. After washing with deionized water to neutralize it, the BC was homogenized to obtain a BC homogenate. Then BC film was prepared by vacuum filtration and dried. With BC as a template, it was immersed in a 0.1 mol/L $AgNO_3$ solution and placed in an autoclave with reaction conditions of 0.1 MPa and 121 °C for a hydrothermal reaction until the beige BC membrane turned brown, proving the successful synthesis of silver nanoparticles.

CAlg encapsulated BC/Ag film: The BC/Ag composite film prepared by the hydrothermal method was dried in an oven to a constant weight and then dipped into a 1% Alg solution. The composite film impregnated with Alg was placed in a 5 wt% $CuCl_2$ coagulation bath to crosslink Alg. The CAlg encapsulated BC/Ag film was obtained after washing with deionized water and drying in an oven at 60 °C for 12 h.

CuS deposition on the CAlg encapsulated BC/Ag composite film: Relying on the copper salt in the CAlg layer, the BC/Ag/CAlg composite film was immersed in a Na_2S solution at a concentration of 0.1 mol/L and sulphurised at 20 °C for 2 min to deposit a layer of CuS in situ on the surface of the composite film, which was removed and washed in deionized water and dried to obtain BC/Ag/CAlg/CuS composite antibacterial film with thermally responsive properties.

Characterization

FTIR spectra of the films were obtained with a Spotlight 400 spectrometer in ambient conditions. An average of 32 scans with a resolution of 4 cm^{-1} in the range of wavelength 650–4000 cm^{-1} was employed in attenuated total reflectance (ATR) mode. X-ray diffraction (XRD) was carried out using a DX-2700BH X-ray diffractometer (PANalytical) with Cu Kα radiation ($\lambda = 1.54$ Å) and a 2θ scanning range of 10–90°. CuS and nano-Ag were tested in powder form, while BC, CAlg, BC/Ag/CAlg/CuS, and BC/Ag samples were tested in thin film form, and all samples were tested in reflection mode. The morphology of the prepared films was characterized by a field emission scanning electron microscope (FESEM) (Quanta-450) operating at an accelerating voltage of 10 kV. SEM samples were all films, which we cut into small 2 mm × 2 mm square pieces and glued to the sample stage by means of carbon glue, as the samples for the SEM investigations were treated with spray-gold. The mechanical properties of the composite films were measured at room temperature (25 °C) at a constant speed of 5 mm/min with a universal testing machine (UM-5504, Sans), each group of films was measured at least 5 times. Water absorption is the mass difference between wet and dry weights divided

by their initial masses. Before immersed the samples in water for 3 h, the test films were dried to a constant weight in a vacuum at 50 °C. Thermogravimetric analysis (TGA, Q500, TA Instruments) was performed from 30 to 800 °C at a heating rate of 10 °C/min under a nitrogen atmosphere. Ultraviolet absorption spectra (UV) were recorded using a Shimadzu UV-2600 spectrometer from 200 to 600 nm. The antibacterial properties of the composite membrane were tested by the plate diffusion method. After coating a 9 and 15 cm diameter solid medium with an active bacterial solution, the test composite membrane sample was placed in the middle of the medium, and the bacteria's growth state was recorded after 3 days. The electrical properties of the films were measured via a four-probe tester (ST2263). An infrared thermographic camera was used to measure the temperature variation and thermographic properties of the films (FLIR ONE Pro).

Results and discussion

Manufacturing of the thermally responsive antimicrobial film

The BC film, with excellent biocompatibility, has been proven to be a suitable substrate for the in situ growth of functional particles. To achieve efficient storage, controlled release, and thermal response of the antimicrobial components of the dressing, we designed a multilayer composite membrane to obtain these functions simultaneously, as shown in Fig. 1. BC membranes were used as templates to generate

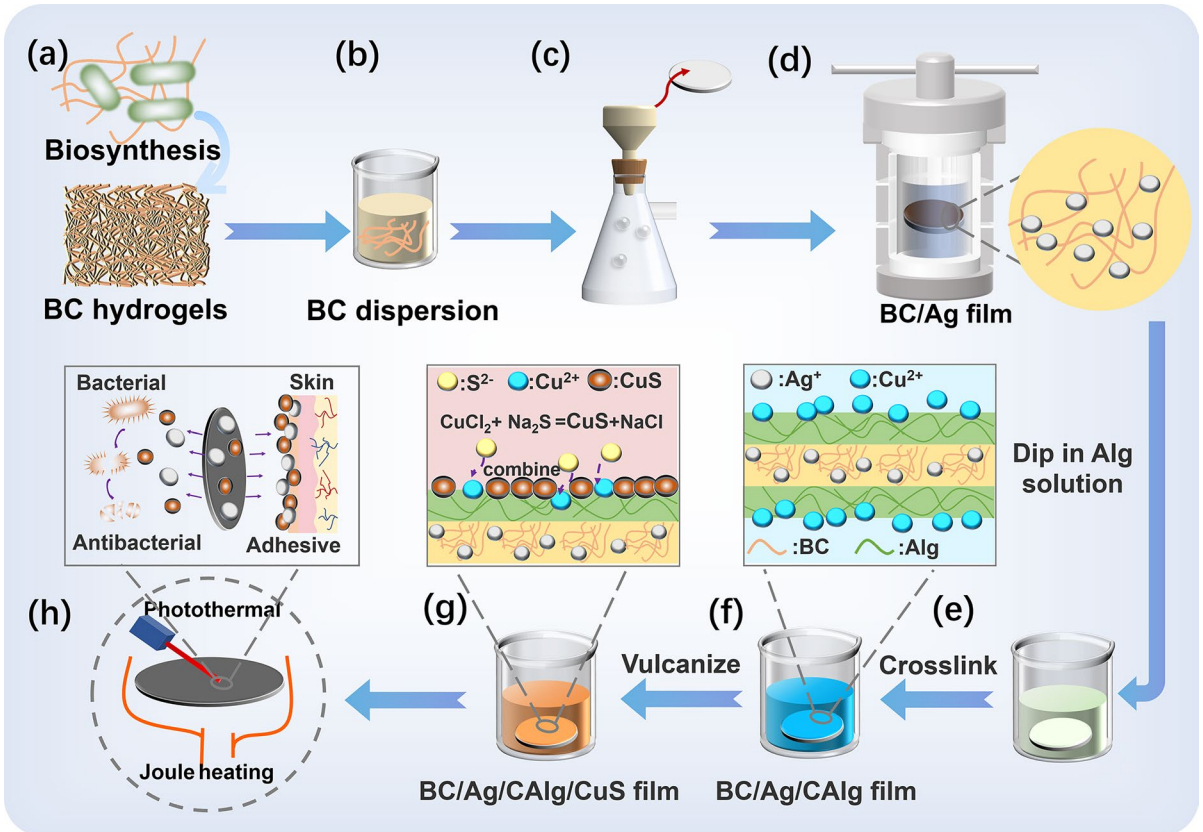

Fig. 1 Schematic diagram of the BC/Ag/CAlg/CuS composite film preparation process **a** BC hydrogel is produced by biosynthesis **b** Dissolution of BC in alkaline solution **c** The BC film was formed by vacuum filtration **d** Growth of Ag on BC film by the hydrothermal method **e** The BC/Ag composite membrane was impregnated with Alg solution **f** Obtained BC/Ag/CAlg composite film by $CuCl_2$ crosslinking **g** A CuS layer forms on the surface of CAlg after curing in a sulfur source **h** Applications include photothermal, electrothermal, wound healing, and bacterial inhibition

silver (Ag) nanoparticles in the BC template structure using a hydrothermal synthesis method in this work. The BC/Ag composite membranes were further impregnated in a sodium alginate (Alg) solution using copper ions to form a copper alginate (CAlg) cladding layer. Based on Cu^{2+} ions in copper alginate, a layer of copper sulfide (CuS) was formed on the surface of the composite antimicrobial film by a liquid-phase sulfide reaction. Finally, we prepared a bright medical dressing with a controlled release of photothermal and electrothermal energy. This composite antibacterial film maintains biocompatibility, degradability, moisture absorption, and water retention, relying on BC and Alg. In the meantime, the material exhibited good photothermal and electrothermal response abilities except for ensuring the excellent antibacterial properties of the composite material owing to the introduction of a CuS layer. Based on the nano-network of BC, the composite antibacterial film presents excellent breathability and oxygen permeability while achieving free exchange of antibacterial copper and silver ions with electrolytes in body fluids.

Microstructure and properties of the composite antimicrobial film

FT-IR analysis can be used to determine the composite film's surface material composition. The stretching vibration absorption band of the hydroxyl group is at approximately 3400 cm^{-1}, the stretching vibration absorption band of the carboxyl anion and glycosidic bond C–O–C is at around 1609 cm^{-1} and 1083 cm^{-1} (Leal et al. 2008; Yang et al. 2022) as shown in Fig. 2a. Silver ions are reduced by BC, which also serves as a stabilizer to stop the resulting Ag nanoparticles from aggregating and a matrix for homogeneous distribution and immobilization during the hydrothermal reduction reaction for Ag formation (Li et al. 2014). When compared to the purified BC curve, which had an absence of the remarkable characteristic band at 1613 cm^{-1}, which indicated that the –OH at C_6 of BC was changed into C=O during the reduction reaction, the BC/Ag curve's great characteristic band at 1613 cm^{-1} indicates the existence of C=O. The infrared curve of the BC/Ag/CAlg/CuS film shows the absorption band of the cross-linked CAlg, attempting to prove that the CAlg forms an interpenetrating structure with BC/Ag sample, and the absorption band of –OH at 3400 cm^{-1} is narrowed, indicating that Alg interacts with -OH on the surface of BC, confirming the above viewpoint again (Yang et al. 2022). Meanwhile, the BC/Ag/CAlg/CuS films, which form the interpenetrating network, still retain water absorption of up to 240%, as shown in Fig. 2c.

To further confirm the presence of nano-silver and CuS particles in composite films, the XRD spectrum in Fig. 2b was used. As shown by the clear absorption bands of the sample nano-silver powder at 38.2°, 44.4°, 64.5°, and 77.5°, which are situated on the (111), (200), (220), and (311) crystal faces of the corresponding cubic silver, the nano-silver possesses a face-centered cubic structure (Jalali et al. 2016; Zhu et al. 2013). Ag was successfully grafted onto BC film through in-situ growth using BC film as a template, as evidenced by the XRD curve of BC/Ag, which displays the absorption band of BC are at 14.7°and 22.7°, which were indexed as the (100) and (110) peaks of cellulose Iα (French 2014) and three absorption bands of Ag (111), (200), and (220). The CuS curve reveals that the (100), (110) and (116) crystal planes of CuS are responsible for the sharp crystallization bands at 31.7°, 48.1° and 58.7°, respectively. The (100) crystal plane of CuS and the (111) crystal plane of Ag appeared in BC/Ag/CAlg/CuS samples at 31.7° and 38.2° respectively (Roy et al. 2020), after cross-linking CAlg vulcanization, indicating that after dipping CAlg, the nano-silver migrated from the inside of the film to the surface of the film, realizing the transfer of nano-silver along the Alg. Furthermore, the BC/Ag/CAlg/CuS sample still shows the absorption band of BC, again proving that CAlg does not entirely cover the surface of BC/Ag but enters the network void of BC, forming a CAlg-BC interpenetration structure. The weight loss ratio of the composite film from the TGA test can also reflect the in situ formation of silver and copper sulfide particles (Fig. 2d) (Fig. S1).

Figure 2e displays the physical morphologies of the various films. Pure BC is a translucent film, and CAlg film is transparent blue-green in the dry state. Due to the in-situ synthesis of silver particles, the BC/Ag film is light brown and opaque, while the BC/Ag/CAlg sample coated with CAlg is a translucent, light green film. This phenomenon should be attributed to the fact that Alg enters the network structure of BC during impregnation and fills the gap while chelating between the alginic acid molecular chain and Cu^{2+} to form an "eggshell structure", which further compacts

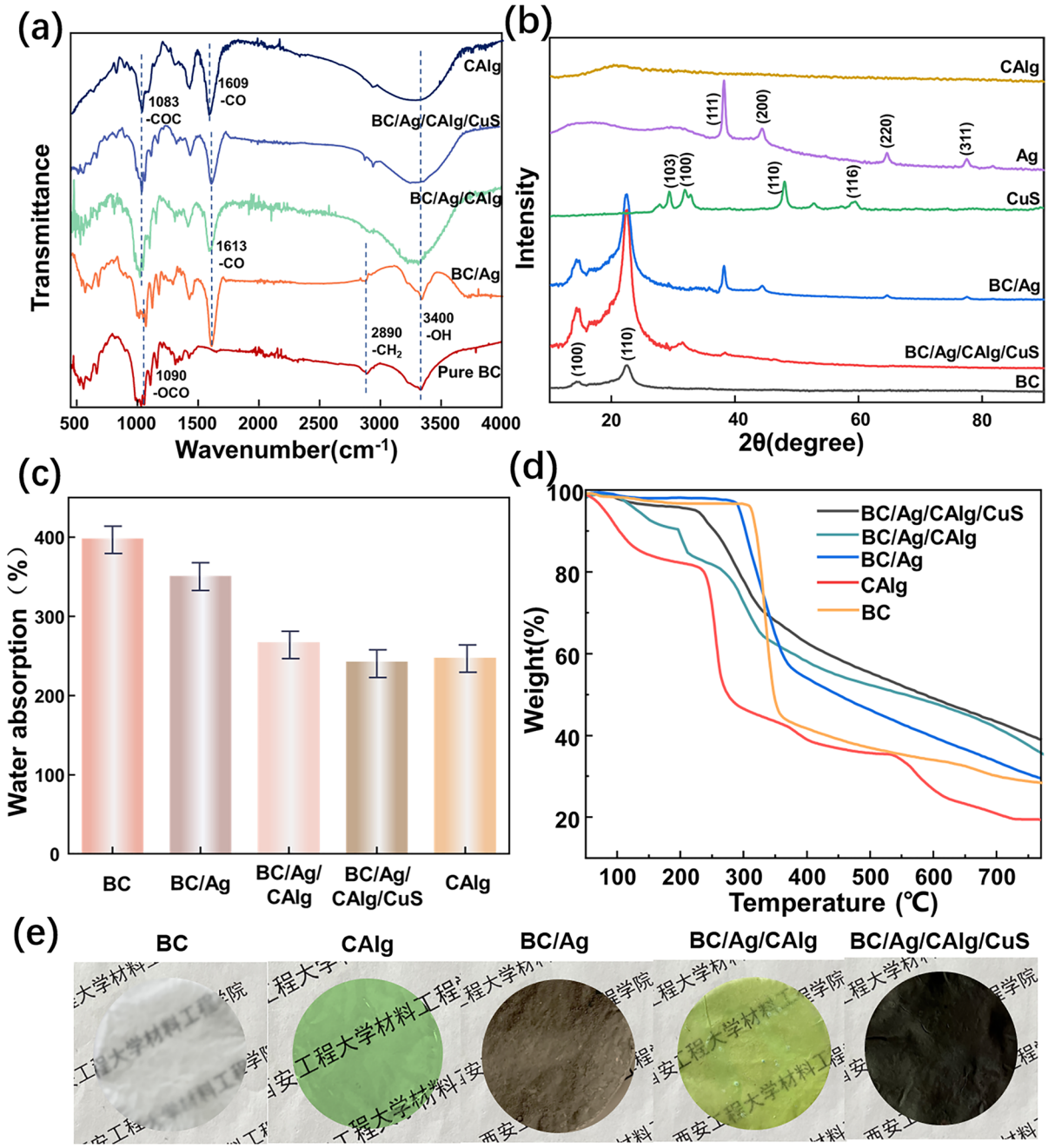

Fig. 2 **a** XRD curves of Ag and CuS powder, BC/Ag/CAlg/CuS film, BC/Ag/CAlg film, BC/Ag film, BC film and CAlg film **b** FTIR curves of BC/Ag/CAlg/CuS film, BC/Ag/CAlg film, BC/Ag film, BC film and CAlg film **c** Water absorption of BC/Ag/CAlg/CuS film, BC/Ag/CAlg film, BC/Ag film, BC film and CAlg film **d** TGA curves of BC/Ag/CAlg/CuS film, BC/Ag/CAlg film, BC/Ag film, BC film and CAlg film **e** Digital image of film characteristics of BC/Ag/CAlg/CuS film, BC/Ag/CAlg film, BC/Ag film, BC film and CAlg film

the internal structure of the film and increases the refractive index of the film, resulting in the translucent state of the film. After CuS deposition, the BC/Ag/CAlg/CuS film turns black.

SEM images show the surface morphology of the composite membranes. Figure 3a shows BC film's unique network structure (Fig. S2). Numerous silver nanoparticles are on the surface of the BC/Ag film after the silver nanoparticles have in situ synthesis, demonstrating the efficacy of the high-temperature, high-pressure hydrothermal process used to create the silver nanoparticles on the BC film (Fig. 3b). The bulge and network structure of the BC/Ag/CAlg samples vanished after CAlg was dip-coated (Fig. 3c). Because sodium alginate is a water-soluble material and BC is a hydrophilic material, the process of coating BC with sodium alginate is realized by impregnation, and the sodium alginate solution can easily swell into the network of BC through water absorption. This smooth surface indicates that CAlg has completely penetrated its network structure, forming a CAlg-BC interpenetrating structure. The film structure becomes denser, confirming that BC/Ag/CAlg samples become transparent (Fig. 2f). As shown in Fig. 3d, a CuS layer is deposited on the surface of the BC/Ag/CAlg/CuS film, providing the premise for a photothermal and electric thermal stimulation response. Through the SEM cross-section image, we can see that Ag particles are distributed in the BC cross-section, which proves Ag's successful synthesis, as shown in Fig. 3f. In Fig. 3g, the BC/Ag/CAlg film comprises several layers, with Alg closely connected, and the boundary is almost indistinguishable. The multi-layer structure with a three-dimensional nanofiber network and the firm connection between layers provide a solid foundation for the excellent comprehensive properties of the film, especially the mechanical properties. This structure makes Ag well embedded in the BC network and effectively enhances the interaction between BC and Alg. However, in Fig. 3h, there are some voids in the BC/Ag/CAlg/CuS sample, which proves that CuS will compete with crosslinked CAlg for Cu^{2+} in the synthesis process so that some copper alginate will be lost after losing Cu^{2+}, thus forming voids. We performed elemental analysis by EDS test to confirm whether nano-silver particles would come out and be lost during the preparation process. Figure 3i shows only two elements, C and O, in the BC film, and Ag elements are uniformly distributed on the surface of the BC/Ag sample, demonstrating the successful synthesis of silver nanoparticles. Because of the Cu^{2+} in the coagulation bath, the element Cu appeared on the EDS image after dipping CAlg. Many elements, including Cu and S, were evenly distributed on the surface of BC/Ag/CAlg/CuS samples after CuS deposition.

Mechanical properties and reinforcing mechanism of BC/Ag/CAlg/CuS composite film

Figure 4a depicts a typical stress-strain curve of a composite film. All films are broken brittlely, with limited elongation at break and no apparent yield, which should be attributed to the rigidity of BC materials and nano-Ag particles. BC film has a maximum tensile strength of 18.4 ± 1.8 MPa. With the addition of nano-Ag particles, the tensile strength reached 20.0 ± 0.9 MPa, and the mechanical strength of BC was not reduced, which was attributed to the strong interaction between polymer matrix and nano-Ag particles and their excellent dispersibility (Table S1). On the other hand, the tensile strength of the BC/Ag/CAlg film decreased, which should be attributed to the lower strength of CAlg, as the tensile strength of CAlg is only 15.1 ± 1.2 MPa. However, the BC/Ag/CAlg/CuS sample has a minor fracture strength of only 14 ± 1.5 MPa compared to the other samples because the Cu^{2+} in the cross-linked CAlg competes with the copper source in the synthetic CuS, and the synthesis of CuS is accompanied by a reduction in CAlg. The above phenomenon analysis demonstrates that CAlg and BC form an interpenetrating structure rather than a coated one. The BC/Ag/CAlg/CuS composite film with a width of 4 mm and a thickness of 0.01 mm, as well as the BC/Ag sample, can easily lift the weight of 50 g (Fig. 4b), demonstrating its application potential in the bandage-type dressing field.

Joule heating and photothermal performance of BC/Ag/CAlg/CuS film

Films made of BC/Ag/CAlg/CuS exhibit good electrothermal stability. The maximum steady-state temperature rises with increased applied voltage, as shown in Fig. 5a. It has adjustable electrothermal performance, when the voltage is supplied to 30 V, the temperature of the sample increases quickly, reaching its maximum value only in 20 s, and declines

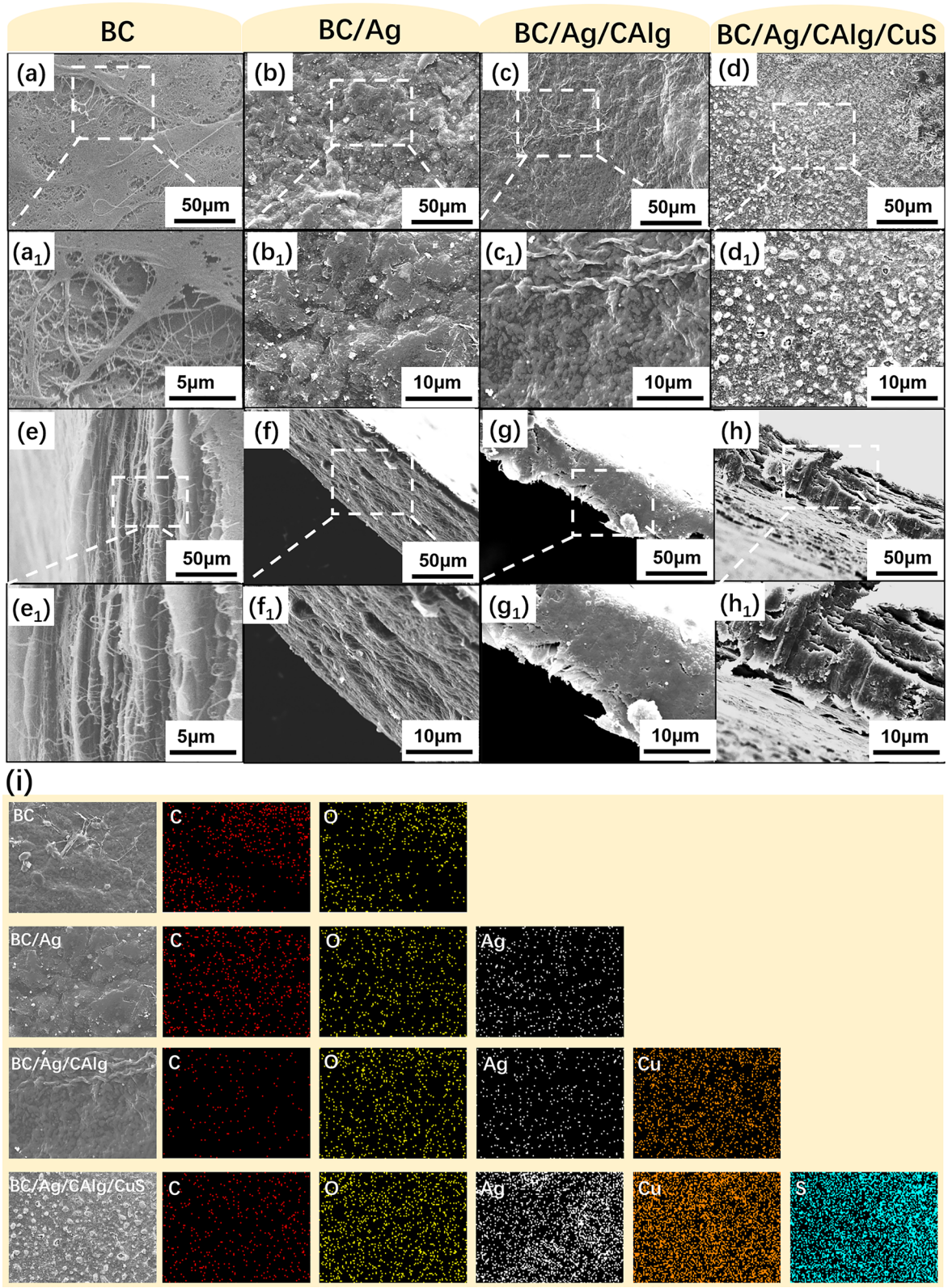
BC
BC/Ag
BC/Ag/CAlg
BC/Ag/CAlg/CuS
(a)
(b)
(c)
(d)
50μm
(a1)
(b1)
(c1)
(d1)
5μm
10μm
(e)
(f)
(g)
(h)
(e1)
(f1)
(g1)
(h1)
(i)
BC
C
O
BC/Ag
Ag
BC/Ag/CAlg
Cu
BC/Ag/CAlg/CuS
S

◂**Fig. 3** **a–e** SEM images for the surface of BC film (a, a_1), BC/Ag film (b, b_1), BC/Ag/CAlg film (c, c_1), and BC/Ag/CAlg/CuS film (d, d_1) CAlg film **e–h** SEM images for the cross-section of BC film (e, e_1), BC/Ag film (f, f_1), BC/Ag/CAlg film (g, g_1), and BC/Ag/CAlg/CuS film (h, h_1) **i** EDS spectra of BC film, BC/Ag film, BC/Ag/CAlg film and BC/Ag/CAlg/CuS film

quickly to room temperature in 40 s when the voltage is switched off. In the linear I-V curve (as shown in Fig. 5b), the BC/Ag film's resistance is low because BC's unique network structure completely covers a small amount of nano-Ag particles. However, after being impregnated with Alg, the resistance of the BC/Ag/CAlg film increases because the molecular chain of Alg enters the BC network, causing nano-Ag particles to migrate from the interior to the surface and thereby increasing the conduct. BC/Ag/CAlg/CuS sample has excellent conductive properties, which make its resistance stable and ensure the safety of electrothermally controlled antibacterial dressing for the human epidermis. Figure 5c characterizes the BC/Ag/CAlg/CuS film electric heating test sample and the related infrared thermal image captured by an infrared thermal imager (IR), clearly showing the heating process and temperature change. These findings demonstrate that BC/Ag/CAlg/CuS films have a fast thermal response, stability, and safety.

The development of controllable, innovative antimicrobial dressings with thermal stimulus-response is essential for the ease of use of functional dressings. Herein, the existence of the CuS layer explains the photothermal performance of BC/Ag/CAlg/CuS composite film. On the one hand, the photothermal properties can achieve the controlled release of antibacterial silver ions. On the other hand, CuS is also an antibacterial material that can achieve a synergistic antibacterial effect. Figure 6a demonstrates the photothermal properties of the composite film in the near-infrared. Adding silver nanoparticles accelerates the heating rate of BC and Ag samples. The temperature quickly rose to 72 °C after applying the CuS layer to the surface. Near-infrared light was used to further demonstrate the excellent photothermal performance of the BC/Ag/CAlg/CuS sample. After irradiation, Fig. 6b shows that the temperature dropped to room temperature in 30 s, and the photothermal effect of the BC/Ag/CAlg/CuS film remained stable after repeated cycles. The temperature change (maximum in the central location) was measured using an infrared thermal imager (Fig. 6c). Under 250 W infrared lamp irradiation, the temperature of BC/Ag/CAlg/CuS film increases linearly, and the temperature of BC/Ag/CAlg/CuS film can quickly rise to 60 °C in 20 s, with a maximum temperature of 72 °C. The CuS layer gives the composite film excellent photothermal performance, including fast response, high sensitivity, intelligent controllability, and safe operation. It has a tremendous impact on the clinical application of photothermal therapy (Ren et al. 2022).

Antibacterial properties of BC/Ag/CAlg/CuS composite film

Since the film dressing will be in direct contact with the skin during application, its slow-release antimicrobial properties are one of its most essential

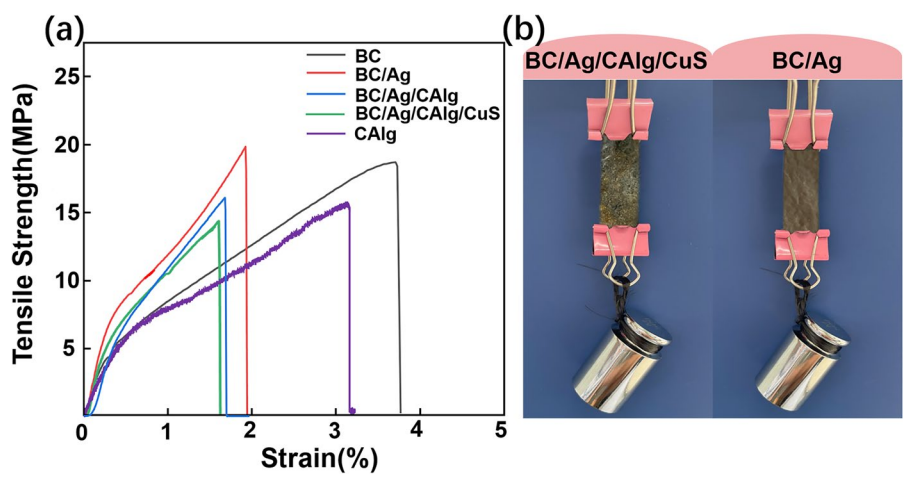

Fig. 4 **a** Stress-strain curves of BC/Ag/CAlg/CuS film, BC/Ag/CAlg film, BC/Ag film, BC film and CAlg film **b** Digital image of 4 mm×10 mm BC/Ag/CAlg/CuS film and BC/Ag film lifts 50 g weight

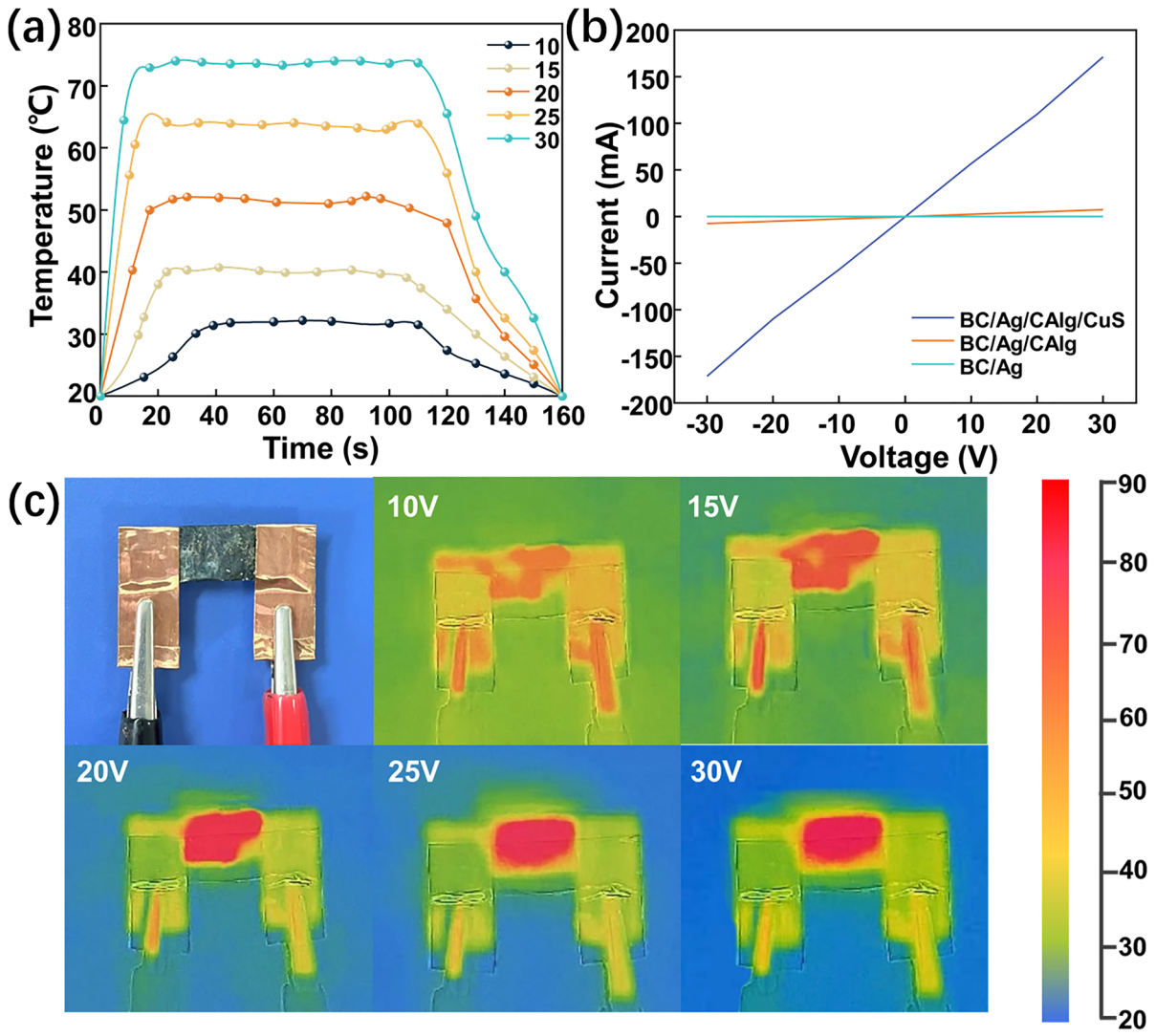

Fig. 5 **a** Temperature plots against time under different voltages for BC/Ag/CAlg/CuS film **b** I–V curve of BC/Ag/CAlg/CuS film, BC/Ag/CAlg film and BC/Ag film **c** Electric heating test sample and the associated infrared thermal images of BC/Ag/CAlg/CuS film

characteristics. Figure 7 shows the mechanism of the effect of thermal stimulation and time on the retardation effect of the samples and UV analysis. UV analysis shows the retardation effect of the samples at the same temperature (20 °C) and different soaking times (12 h, 24 h, 36 h), as in Fig. 7b, and simultaneously (12 h) and at different soaking temperatures (36 °C, 50 °C, 60 °C). The results showed that the higher the photothermal temperature and the longer the impregnation time, the higher the absorbance of the leachate.

AgNPs have good antibacterial activity, as shown in Fig. 8a, with 99.9% activity against *E. coli* and *S. aureus*. It works through three antibacterial mechanisms: (1) When positively charged silver ions come into contact with negatively charged microbial cells, they adsorb to each other. (2) Silver ions pierce the cell surface, destroy cell DNA, inhibit protein formation, and prevent cell metabolism and reproduction until death, thus achieving bactericidal effects. (3) When the cells become inactive, the silver ions leave

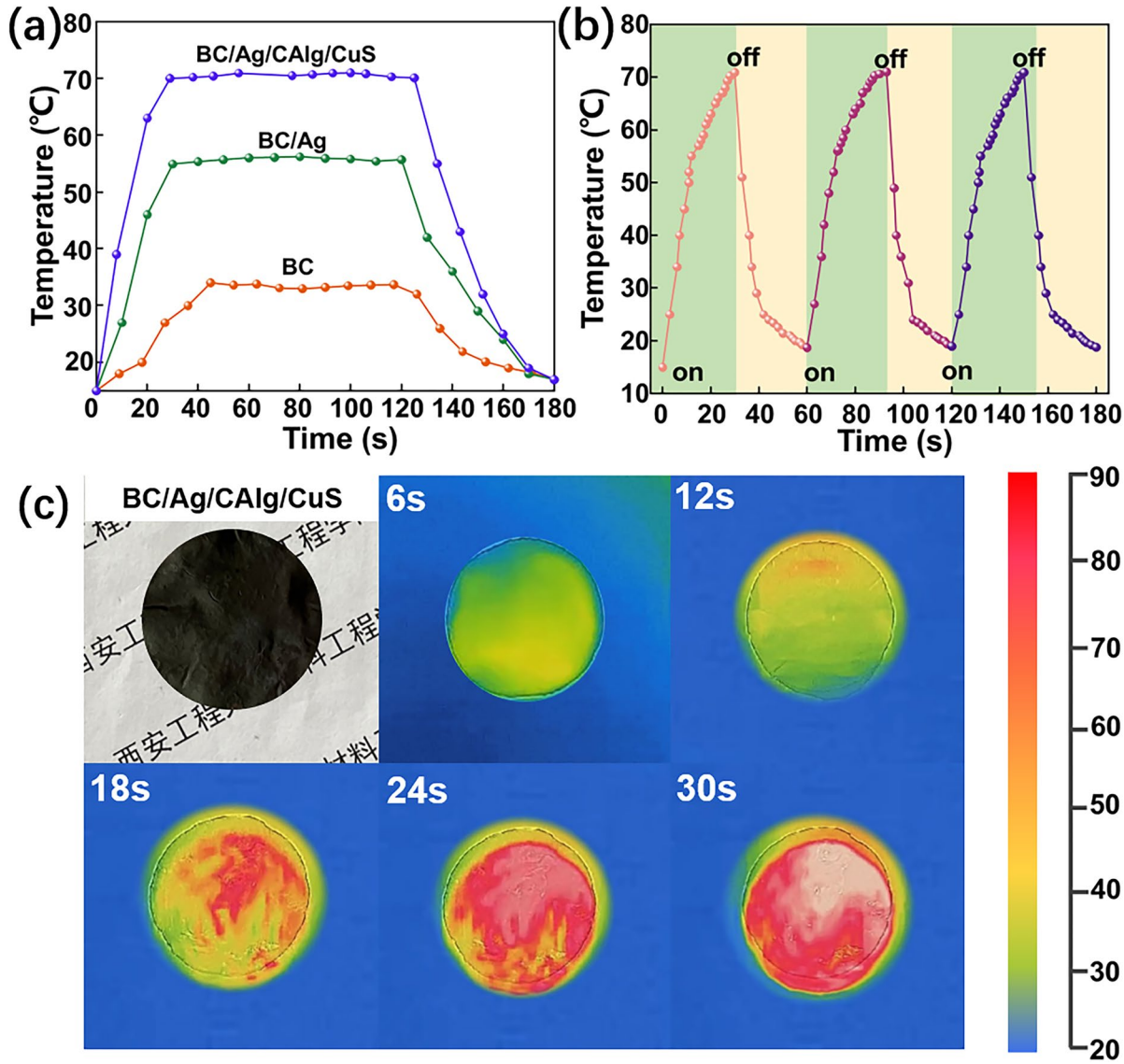

Fig. 6 **a** Surface temperature-time curves of BC/Ag/CAlg/CuS film, BC/Ag film and BC film under 250 W near-infrared light **b** Surface temperature-time curve of BC/Ag/CAlg/CuS film under repeated heating/cooling cycles **c** Optical and IR images of the surfaces of BC/Ag/CAlg/CuS film under 250 W near-infrared light for different time

and resist the bacteria, resulting in a long-lasting, non-toxic antibacterial effect (Korshed et al. 2018; Li et al. 2013). BC films do not have any antibacterial properties. The antibacterial rate of BC/Ag films against *E. coli* and *S. aureus* can be increased up to 74.5% and 79.8% by tracing AgNPs and the antibacterial properties of BC/Ag/CAlg samples due to Cu^{2+} cross-linking in Fig. 8b. NIR light did not affect the inhibition rate of the above samples. However, Fig. 8c shows that the antibacterial activity of CuS was significantly enhanced to 99.7% when exposed to 250 W of NIR light, indicating a significant photothermal antibacterial effect of CuS. CuS converts light energy into heat energy by irradiating the photothermal agent with a specific wavelength of light. The temperature increase weakens bacterial tolerance and kills bacteria at high temperatures. The BC/Ag/CAlg/CuS films showed 99.9% and 99.6% inhibition against *S. aureus* and *E.*

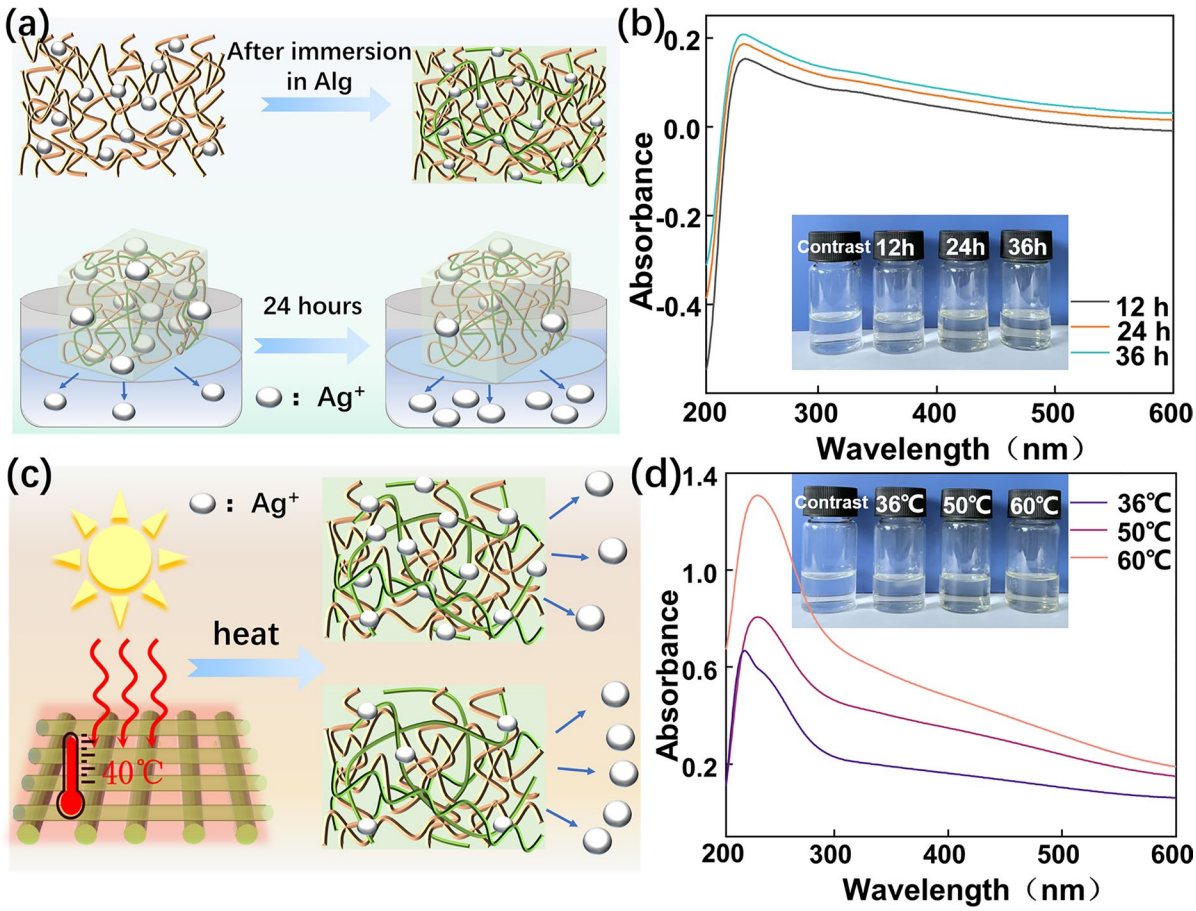

Fig. 7 **a** Sustained release mechanism of BC/Ag/CAlg/CuS film in isothermal **b** UV analysis after dressing soaking for 12 h, 24 h, and 36 h in isothermal **c** Sustained release mechanism of BC/Ag/CAlg/CuS film in isochronism **d** UV analysis after dressing soaking for 36 °C, 50 °C, 60 °C in isochronism

coli due to the synergistic effect of the electric and light-heat stimulation responses of Ag ions and CuS in Fig. 8d. Furthermore, the outer electrothermal or photothermal effect of CuS will raise the temperature of the film, which can promote the release of internal Ag while inhibiting bacteria. The antibacterial rate also can be further controlled by controlling the electrothermal or photothermal temperature, resulting in an intelligent and controllable antibacterial of the film.

Conclusions

Based on the nano-network of BC and the interpenetrating structure formed between BC and CAlg, this work created a copper alginate-encapsulated BC/Ag composite antibacterial film with thermally responsive properties. This structural design gave the composite antibacterial film good biocompatibility, moisture absorption, and breathability. Adding a CuS layer endowed the photothermal and electrothermal response of the composite film while maintaining its excellent antibacterial properties. The BC/Ag/CAlg/CuS composite film inhibited *S. aureus* and *E. coli* up to 99.9% and 99.6%, respectively. The controlled release of antibacterial ions from the composite film material is made possible by the dual photothermal and electrothermal stimulation responses and the synergistic antibacterial functions of CuS and Ag ions. This work opens up new possibilities for using and developing advanced dressings.

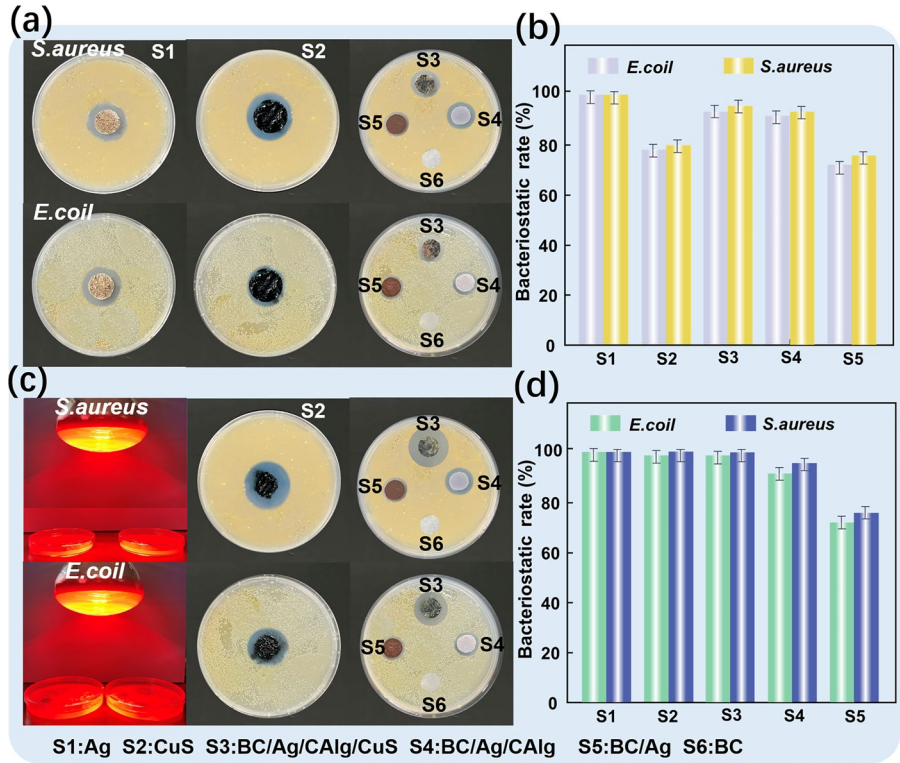

Fig. 8 **a** Agar plate diffusion method was used to test the bactericidal performance of AgNPs powder, CuS powder, BC/Ag/CAlg/CuS film, BC/Ag/CAlg film, BC/Ag film and BC film against *E. coli* and *S. aureus* in the natural environment **b** Bacterial inhibition rate of AgNPs powder, CuS powder, BC/Ag/CAlg/CuS film, BC/Ag/CAlg film, BC/Ag film and BC film against *E. coli* and *S. aureus* in natural environment **c** Agar plate diffusion method was used to test the bactericidal performance of AgNPs powder, CuS powder, BC/Ag/CAlg/CuS film, BC/Ag/CAlg film, BC/Ag film and BC film against *E. coli* and *S. aureus* under 250 W near-infrared light irradiation **d** Bacterial inhibition rate of AgNPs powder, CuS powder, BC/Ag/CAlg/CuS film, BC/Ag/CAlg film, BC/Ag film and BC film against *E. coli* and *S. aureus* under 250 W near infrared light

Acknowledgments Not applicable.

Author contributions BS, TZ, XL and KY carried out the experiment as well as the test characterization. GT and YD provided assistance in conceiving experiments and analyzing data. JM conceived the idea and designed the experiments. All the authors have approved the final version of the manuscript.

Funding This study was funded by the National Natural Science Foundation of China (51903198), Key Research and Development Program of Shaanxi (No. S2022-YF-YBNY-0187), Scientific Research Program Funded by Shaanxi Provincial Education Department (20JY025), Natural Science Basic Research Program of Shaanxi (No. 2022JQ-775), Health Scientific Research project of Shaanxi Province (No.2022E020), Young Talents Fund of Association for Science and Technology in Shaanxi (No. SWYY202210), 2021 China National Textile and Apparel Council(CNTAC)Science and Technology Guidance Program (2021007). 2023 Graduate Innovation Fund Project of Xi'an Engineering University (chx2022030).

Data availability Not applicable.

Declarations

Conflict of interest The authors declare no competing interests.

Consent for publication Informed consent was obtained from all individual participants included in the study.

Ethical approval All procedures performed in studies involving human participants were in accordance with the ethical standards of the institutional and/or national research committee and with the 1964 Helsinki declaration and its later amendments or comparable ethical standards.

References

Chiaoprakobkij N, Sanchavanakit N, Subbalekha K, Pavasant P, Phisalaphong M (2011) Characterization and biocompatibility of bacterial cellulose/alginate composite sponges with human keratinocytes and gingival fibroblasts. Carbohydr Polym 85(3):548–553. https://doi.org/10.1016/j.carbpol.2011.03.011

Dart A, Bhave M, Kingshott P (2019) Antimicrobial peptide-based electrospun fibers for wound healing applications. Macromol Biosci 19:1800488. https://doi.org/10.1002/mabi.201800488

Deng XY, Huang BX, Wang QH, Wu WL, Coates P, Sefat F, Lu CH, Zhang W, Zhang XM (2021) A mussel-inspired antibacterial hydrogel with high cell affinity, toughness, self-healing, and recycling properties for wound healing. ACS Sustain Chem Eng 9(8):3070–3082. https://doi.org/10.1021/acssuschemeng.0c06672

Dos Santos C, Seckler MM, Ingle A, Gupta I, Galdiero S, Galdiero M, Gade A, Rai M (2014) Silver nanoparticles: therapeutical uses, toxicity, and safety issues. J Pharm Sci 103(7):1931–1944. https://doi.org/10.1002/jps.24001

Durand AG, Raoult D, Dubourg G (2019) Antibiotic discovery: history, methods and perspectives. Int J Antimicrob Agents 53:371–382. https://doi.org/10.1016/j.ijantimicag.2018.11.010

French AD (2014) Idealized powder diffraction patterns for cellulose polymorphs. Cellulose 21(2):885–896. https://doi.org/10.1007/s10570-013-0030-4

Jalali S, Allafchian A (2016) Assessment of antibacterial properties of novel silver nanocomposite. J Taiwan Inst Chem Eng 59:506–513. https://doi.org/10.1016/j.jtice.2015.08.004

Ji L, Zhang FL, Zhu LW, Jiang JX (2021) An in-situ fabrication of bamboo bacterial cellulose/sodium alginate nanocomposite hydrogels as carrier materials for controlled protein drug delivery. Int J Biol Macromol 170:459–468. https://doi.org/10.1016/j.ijbiomac.2020.12.139

Jiang Y, Yu GB, Zhou Y, Liu YY, Feng YH, Li JC (2020) Effects of sodium alginate on microstructural and properties of bacterial cellulose nanocrystal stabilized emulsions. Colloid Surf A 607:125474. https://doi.org/10.1016/j.colsurfa.2020.125474

Korshed P, Li L, Ngo DT, Wang T (2018) Effect of storage conditions on the long-term stability of bactericidal effects for laser generated silver nanoparticles. Nanomaterials 8(4):218. https://doi.org/10.3390/nano8040218

Leal D, Matsuhiro B, Rossi M, Caruso F (2008) FT-IR spectra of alginic acid block fractions in three species of brown seaweeds. Carbohydr Res 343(2):308–316. https://doi.org/10.1016/j.carres.2007.10.016

Lee HY, Park HK, Lee YM, Kim K, Park SB (2007) A practical procedure for producing silver nanocoated fabric and its antibacterial evaluation for biomedical applications. Chem Commun 28:2959–2961. https://doi.org/10.1039/b703034g

Li Z, Wang L, Chen S, Feng C, Chen SY, Yin N, Yang JX, Wang HP, Xu YM (2014) Facilely green synthesis of silver nanoparticles into bacterial cellulose. Cellulose 22(1):373–383. https://doi.org/10.1007/s10570-014-0487-9

Li Y, Zhang W, Niu JF, Chen YS (2013) Surface-coating-dependent dissolution, aggregation, and reactive oxygen species (ROS) generation of silver nanoparticles under different irradiation conditions. Environ Sci Technol 47(18):10293–10301. https://doi.org/10.1021/es400945v

Liu Y, Wang SS, Wang ZP, Yao QF, Fang SS, Zhou XF, Yuan X, Xie JP (2020) In-situ synthesis of silver nanoclusters inside bacterial cellulose hydrogel for antibacterial application. J Mater Chem B. https://doi.org/10.1039/d0tb00073f

Mutalik C, Okoro G, Krisnawati D, Jazidie A, Rahmawati E, Rahayu D, Kuo T (2022) Copper sulfide with morphology-dependent photodynamic and photothermal antibacterial activities. J Colloid Interface Sci 607:1825–1835. https://doi.org/10.1016/j.jcis.2021.10.019

Nie X, Wu S, Huang F, Li W, Qiao H, Wang Q, Wei Q (2021a) Dew-of-Leaf structure multiple synergetic antimicrobial modality hybrid: a rapid and long lasting bactericidal material. Chem Eng J 416:129072

Nie X, Wu S, Huang F, Wang Q, Wei Q (2021b) Smart textiles with self-disinfection and photothermochromic effects. ACS Appl Mater Interfaces 13(2):2245–2255. https://doi.org/10.1021/acsami.0c18474

Nie X, Wu S, Liao S, Chen J, Huang F, Li W, Wei Q (2021c) Light-driven self-disinfecting textiles functionalized by PCN-224 and Ag nanoparticles. J Hazard Mater 416:125786

Pal S, Nisi R, Stoppa M, Licciulli A (2017) Silver-functionalized bacterial cellulose as antibacterial membrane for wound-healing applications. ACS Omega 2(7):3632–3639. https://doi.org/10.1021/acsomega.7b00442

Pazyar N, Yaghoobi R, Rafiee E, Mehrabian A, Feily A (2014) Skin wound healing and phytomedicine: a review. Skin Pharmacol Physiol 27(6):303–310. https://doi.org/10.1159/000357477

Perotti GF, Barud HS, Messaddeq Y, Ribeiro S, Constantino VRL (2011) Bacterial cellulose–laponite clay nanocomposites. Polymer 52(1):157–163. https://doi.org/10.1016/j.polymer.2010.10.062

Pinto RJB, Marques PAAP, Neto CP, Trindade T, Daina S, Sadocco P (2009) Antibacterial activity of nanocomposites of silver and bacterial or vegetable cellulosic fibers. Acta Biomater 5(6):2279–2289. https://doi.org/10.1016/j.actbio.2009.02.003

Qiao Y, Ping Y, Zhang HB, Zhou B, Liu F, Zhou M (2019) Laser-activatable CuS nanodots to treat multidrug-resistant bacteria and release copper ion to accelerate healing of infected chronic nonhealing wounds. ACS Appl Mater Interfaces 11(4):3809–3822. https://doi.org/10.1021/acsami.8b21766

Ren YW, Yan BB, Wang P, Yu YY, Cui L, Zhou M, Wang Q (2022) Construction of a rapid photothermal antibacterial silk fabric via QCS-guided in situ deposition of CuSNPs. ACS Sustain Chem Eng 10(6):2192–2203. https://doi.org/10.1021/acssuschemeng.1c07758

Rieger KA, Cho HJ, Yeung HF, Fan W, Schiffman JD (2016) Antimicrobial activity of silver ions released from zeolites immobilized on cellulose nanofiber mats. ACS Appl

Mater Interfaces 8(5):3032–3040. https://doi.org/10.1021/acsami.5b10130
Roy S, Rhim JW (2020) Effect of CuS reinforcement on the mechanical, water vapor barrier, UV-light barrier, and antibacterial properties of alginate-based composite films. Int J Biol Macromol 164:37–44. https://doi.org/10.1016/j.ijbiomac.2020.07.092
Shen JF, Dai Y, Xia F, Zhang XJ (2022) Role of divalent metal ions in the function and application of hydrogels. Prog Polym Sci 135:101622. https://doi.org/10.1016/j.progpolymsci.2022.101622
Siddhan P, Sakthivel K, Basavaraj H (2016) Biosynthesis of bacterial cellulose imparting antibacterial property through novel bio-agents. Res J Biotechnol 11:9
Song S, Liu Z, Abubaker MA, Ding L, Zhang J, Yang SR, Fan ZJ (2021b) Antibacterial polyvinyl alcohol/bacterial cellulose/nano-silver hydrogels that effectively promote wound healing. Mater Sci Eng C Mater 126:112171
Song Q, Wei L, Sun J (2021a) Optimal process of electrostatic spinning polyvinyl alcohol/sodium alginate composite nanofiber membranes. Basic Sci J Text Univ 34(1):7–14. https://doi.org/10.13338/j.issn.1006-8341.2021.01.002
Su CH, Kumar GV, Adhikary S, Velusamy P, Pandian K, Anbu P (2017) Preparation of cotton fabric using sodium alginate-coated nanoparticles to protect against nosocomial pathogens. BEJ 117:28–35. https://doi.org/10.1016/j.bej.2016.10.020
Sulaeva I, Henniges U, Rosenau T, Potthast A (2015) Bacterial cellulose as a material for wound treatment: properties and modifications. A review. Biotechnol Adv 33(8):1547–1571. https://doi.org/10.1016/j.biotechadv.2015.07.009
Tabaii MJ, Emtiazi G (2018) Transparent nontoxic antibacterial wound dressing based on silver nano particle/bacterial cellulose nano composite synthesized in the presence of tripolyphosphate. J Drug Deliv Sci Technol 44:244–253. https://doi.org/10.1016/j.jddst.2017.12.019
Wan YZ, Yang SS, Wang J, Gan DQ, Gama M, Yang ZW, Zhu Y, Yao FL, Luo HL (2020) Scalable synthesis of robust and stretchable composite wound dressings by dispersing silver nanowires in continuous bacterial cellulose. Compos B Eng 199:108259. https://doi.org/10.1016/j.compositesb.2020.108259
Wang QQ, Zhang L, Liu YY, Zhang GQ, Zhu P (2020) Characterization and functional assessment of alginate fibers prepared by metal-calcium ion complex coagulation bath. Carbohydr Polym 232:115693. https://doi.org/10.1016/j.carbpol.2019.115693
Wen YY, Yu B, Zhu Z, Yang ZJ, Yang ZR, Shao W (2020) Synthesis of antibacterial gelatin/sodium alginate sponges and their antibacterial activity. Polymers 12(9):1926. https://doi.org/10.3390/polym12091926
Wijnhoven S, Peijnenburg W, Herberts C, Hagens W, Oomen A, Heugens E, Roszek B, Bisschops J, Gosens I, Meent D, Dekkers S, Jong W, Zijverden M, Sips A, Geertsma R (2009) Nano-silver—a review of available data and knowledge gaps in human and environmental risk assessment. Nanotoxicology 3(2):109–138. https://doi.org/10.1080/17435390902725914
Yang G, Xie J, Deng Y, Bian Y, Hong F (2012a) Hydrothermal synthesis of bacterial cellulose/AgNPs composite: a green route for antibacterial application. Carbohydr Polym 87(4):2482–2487. https://doi.org/10.1016/j.carbpol.2011.11.017
Yang G, Xie JJ, Hong F, Cao ZJ, Yang XX (2012b) Antimicrobial activity of silver nanoparticle impregnated bacterial cellulose membrane: effect of fermentation carbon sources of bacterial cellulose. Carbohyd Polym 87(1):839–845. https://doi.org/10.1016/j.carbpol.2011.08.079
Yang G, Yao YQ, Wang CX (2017) Green synthesis of silver nanoparticles impregnated bacterial cellulose-alginate composite film with improved properties. Mater Lett 209:11–14. https://doi.org/10.1016/j.matlet.2017.07.097
Yang HB, Liu ZX, Yin CH, Guan QF, Zhao YX, Ling ZC, Liu HC, Yang KP, Sun WB, Yu SH (2022) Edible, ultrastrong, and microplastic-free bacterial cellulose-based straws by biosynthesis. Adv Funct Mater 32(15):2111713. https://doi.org/10.1002/adfm.202111713
Zhao XH, Li Q, Ma XM, Quan FY, Wang JP, Xia YZ (2015) The preparation of alginate–AgNPs composite fiber with green approach and its antibacterial activity. J Ind Eng Chem 24(2015):188–195. https://doi.org/10.1016/j.jiec.2014.09.028
Zheng L, Li SS, Luo JW, Wang XY (2020) Latest advances on bacterial cellulose-based antibacterial materials as wound dressings. Front Bioeng Biotechnol 8:593768. https://doi.org/10.3389/fbioe.2020.593768
Zhu ZJ, Su M, Ma L, Liu DJ, Wang ZX (2013) Preparation of graphene oxide–silver nanoparticle nanohybrids with highly antibacterial capability. Talanta 117:449–455. https://doi.org/10.1016/j.talanta.2013.09.017